Asynchronous division by non-ring FtsZ in the gammaproteobacterial symbiont of Robbea hypermnestra

Leisch, N.; Pende, N.; Weber, P.M.; Gruber-Vodicka, H.R.; Verheul, J.; Vischer, N.O.E.; Abby, S.S.; Geier, B.; den Blaauwen, T.; Bulgheresi, S.

DOI
10.1038/nmicrobiol.2016.182

Publication date
2016

Document Version
Final published version

Published in
Nature Microbiology

nature microbiology

BRIEF COMMUNICATION

PUBLISHED: 10 OCTOBER 2016 | VOLUME: 2 | ARTICLE NUMBER: 16182

Asynchronous division by non-ring FtsZ in the gammaproteobacterial symbiont of *Robbea hypermnestra*

Nikolaus Leisch[1,2], Nika Pende[1], Philipp M. Weber[1], Harald R. Gruber-Vodicka[2], Jolanda Verheul[3], Norbert O. E. Vischer[3], Sophie S. Abby[1], Benedikt Geier[2], Tanneke den Blaauwen[3] and Silvia Bulgheresi[1]*

The reproduction mode of uncultivable microorganisms deserves investigation as it can largely diverge from conventional transverse binary fission. Here, we show that the rod-shaped gammaproteobacterium thriving on the surface of the *Robbea hypermnestra* nematode divides by FtsZ-based, non-synchronous invagination of its poles—that is, the host-attached and fimbriae-rich pole invaginates earlier than the distal one. We conclude that, in a naturally occurring animal symbiont, binary fission is host-oriented and does not require native FtsZ to polymerize into a ring at any septation stage.

Even though most environmental bacteria are non-culturable and experimentally unappealing, their reproductive modes are compelling as they may challenge well-rooted tenets of bacterial cell biology[1–3]. Model bacteria double in size and divide into two equal daughter cells by a process called binary fission. The highly conserved prokaryotic tubulin homologue FtsZ—a guanosine triphosphatase—plays a central role in the division of many bacteria, archaea and plastids[4]. It initiates cell division by polymerizing into short linear protofilaments, forming the so-called Z-ring underneath the cytoplasmic membrane[5,6]. The Z-ring provides the location of the division site and recruits additional division proteins to form the divisome[7,8]. *In vitro*, the Z-ring has been shown to generate a constrictive force that supposedly allows inward movement (invagination) of the cell envelope during cytokinesis[9,10]. Although ring constriction has long been thought to limit cytokinesis progression, cell wall synthesis and chromosome segregation are currently regarded as the limiting factors of cytokinesis[11]. Two models have been proposed to explain how the Z-ring is formed from FtsZ protofilaments[8]. The 'lateral interaction' model postulates that the Z-ring is a single continuous ring, stabilized by direct lateral interactions between FtsZ protofilaments[12,13], whereas the 'patchy band' model posits that short protofilaments are arranged in a discontinuous band at midcell, without strong lateral contact (for a review see ref. 14). This high-resolution microscopy-based model is also consistent with the FtsZ localization pattern described by fluorescence microscopy for the rod-shaped symbiont of the marine nematode *Laxus oneistus* (referred to as 'Los' from here on). This gammaproteobacterium widens instead of lengthening, and divides via FtsZ-based fission along its long axis, by default[1]. In immunostained dividing cells, FtsZ appears as an elliptical, discontinuous ring at most division stages[1]. Although neither the lateral interaction nor the patchy band model has been conclusively proven, the consensus in all reported studies on the microscale localization pattern of FtsZ is that FtsZ localizes simultaneously and in one clearly recognizable septation plane (or band) at midcell.

To understand whether synchronicity of membrane invagination is essential for FtsZ-based bacterial division, we described the septation of the symbiont of *Robbea hypermnestra* (Supplementary Fig. 1), a nematode closely related to *L. oneistus*[15,16]. Like Los, this symbiont (hereon referred to as Rhs) belongs to a clade of symbiotic Gammaproteobacteria related to the Chromatiaceae and, similarly, it attaches with one pole to the cuticle of its host (Fig. 1a–e). Full-cycle rRNA analysis showed that each *R. hypermnestra* worm is coated by a single bacterial phylotype of Rhs, which are chemosynthetic sulfur-oxidizing bacteria[15]. Growth by widening of the rod-shaped bacterium attached to the cuticle of the nematode *R. hypermnestra* has been hypothesized previously[15] and is shown here by ultrastructural and morphometric analyses (Supplementary Fig. 2a–j). Ultrastructural analysis of Rhs cells dissociated from the nematode (Supplementary Fig. 2a–d) revealed that in Rhs, as in Los[1], septation starts at the poles, progresses along the long axis and gives rise to two identical daughter cells. In contrast to Los, however, Rhs membrane invagination does not proceed synchronously at both poles. As confirmed by ultrastructural analysis of nematode-attached Rhs cells (Fig. 1a–e), the membrane of the proximal (host-attached) pole is always more invaginated than the membrane of the distal pole ($n = 840$, 32% dividing cells; non-dividing cells = 566, proximally invaginated cells = 85, proximally and distally invaginated cells = 189). This indicates that Rhs longitudinal fission starts proximally and proceeds distally, and suggests host-oriented polarization of the bacterial symbiont.

Given the reported role of fimbriae in mediating the attachment of pathogenic Gammaproteobacteria to animal cells[17–19], we applied an antibody against *Escherichia coli* fimbriae (pili) on fixed Rhs cells. In immunostained Rhs cells, the fimbrial signal is asymmetrically localized at the Rhs proximal pole, irrespective of the cell cycle stage (Fig. 1f–i; Supplementary Figs 3a and 4a–f). Asymmetric fimbriae localization at the Rhs proximal pole indicates host-oriented polarization of the symbiont, and suggests fimbriae-mediated symbiont attachment. Fimbriae are proteinaceous and filamentous surface structures that play key roles in infection, as they allow bacteria to adhere, colonize and/or invade host cells[20,21]. In the case of Gram-negative fimbriae, attachment occurs via highly specific interactions with host glycosylated proteins or lipids[22–24]. To our knowledge, Rhs is the first bacterial symbiont displaying asymmetric

[1]Department of Ecogenomics and Systems Biology, Archaeal Biology and Ecogenomics Division, University of Vienna, Althanstrasse 14, 1090 Vienna, Austria. [2]Max Planck Institute for Marine Microbiology, Celsiusstrasse 1, D-28359 Bremen, Germany. [3]Bacterial Cell Biology, Swammerdam Institute of Life Sciences, Faculty of Science, University of Amsterdam, Boelelaan 1108, 1081 HZ Amsterdam, Netherlands. *e-mail: silvia.bulgheresi@univie.ac.at

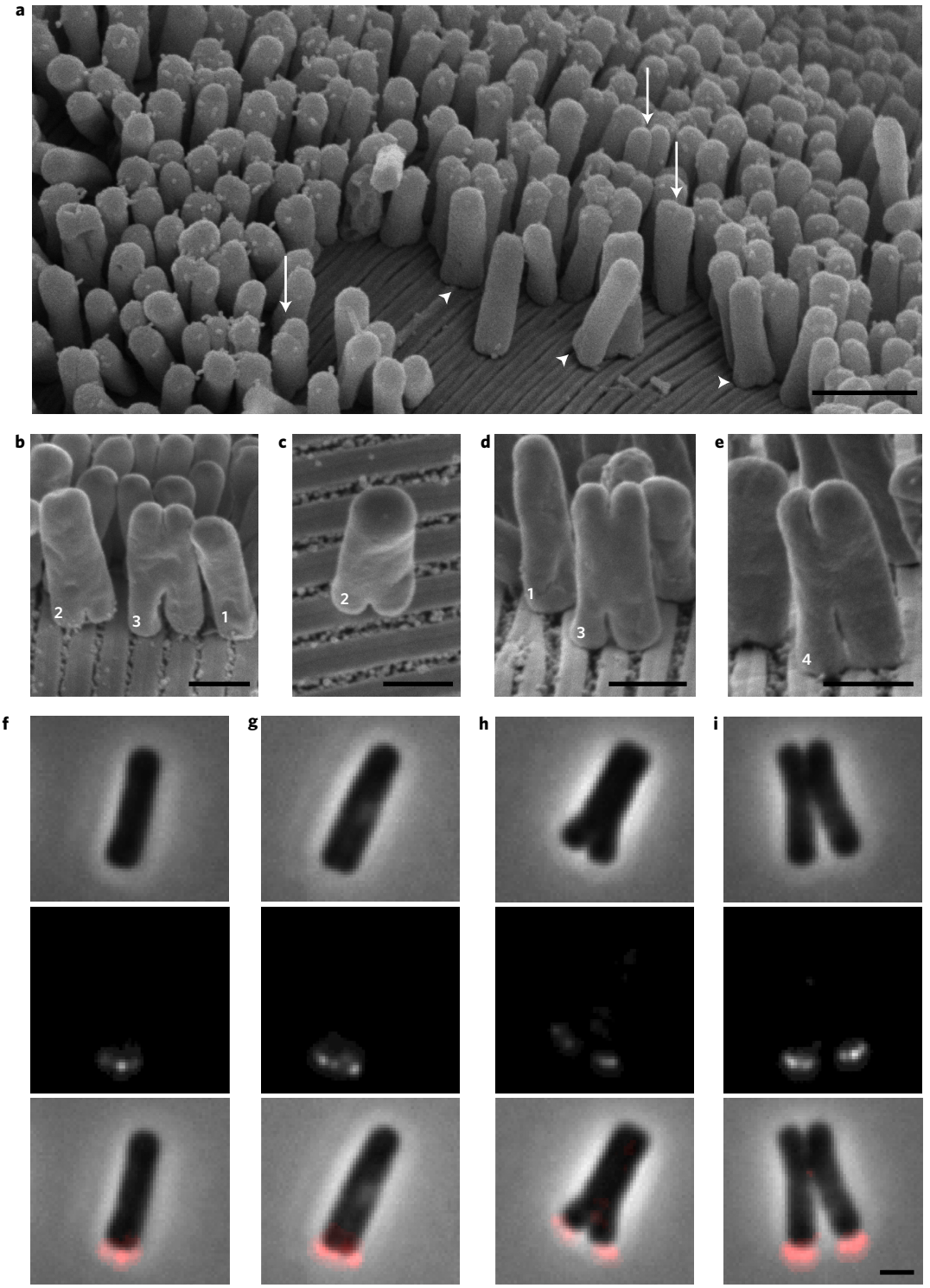

Figure 1 | Asynchronicity of Rhs cell fission and polarity. Representative scanning electron microscopy (SEM) images of the rod-shaped symbiont cells attached to the nematode cuticle and representative phase contrast micrographs of Rhs cells. **a**, Rhs cells are arranged in a monolayer. Arrowheads indicate proximally only invaginated cells, and arrows point to cells with invaginated proximal and distal poles. Scale bar, 5 μm. **b–e**, SEM images of single symbiont cells attached to the nematode cuticle. Different cell cycle stages are indicated with ascending numbers: (1) non-dividing cell; (2) proximally invaginated cell; (3) proximally and distally invaginated cell; (4) cell undergoing the final stage of division. The results are representative of a minimum of ten independent experiments. Scale bar, 1 μm. **f–i**, Top, representative phase contrast micrographs of Rhs cells ordered from early (left) to late (right) stages of the cell cycle and oriented with the proximal cell pole downwards; middle, epifluorescence micrographs of corresponding cells immunostained with anti-fimbriae antibody; and bottom, overlays of phase contrast and epifluorescence (false coloured in red). The results are representative of a minimum of four independent experiments. Scale bar, 1 μm.

localization of fimbriae at the host-attachment site. This is striking, especially in view of the fact that the nematode cuticle is acellular and *de facto* outside the animal body.

To assess whether Rhs longitudinal cell division is FtsZ-based, we cloned and sequenced the Rhs *ftsZ* gene, confirmed its expression by probing membrane-immobilized Rhs protein extracts

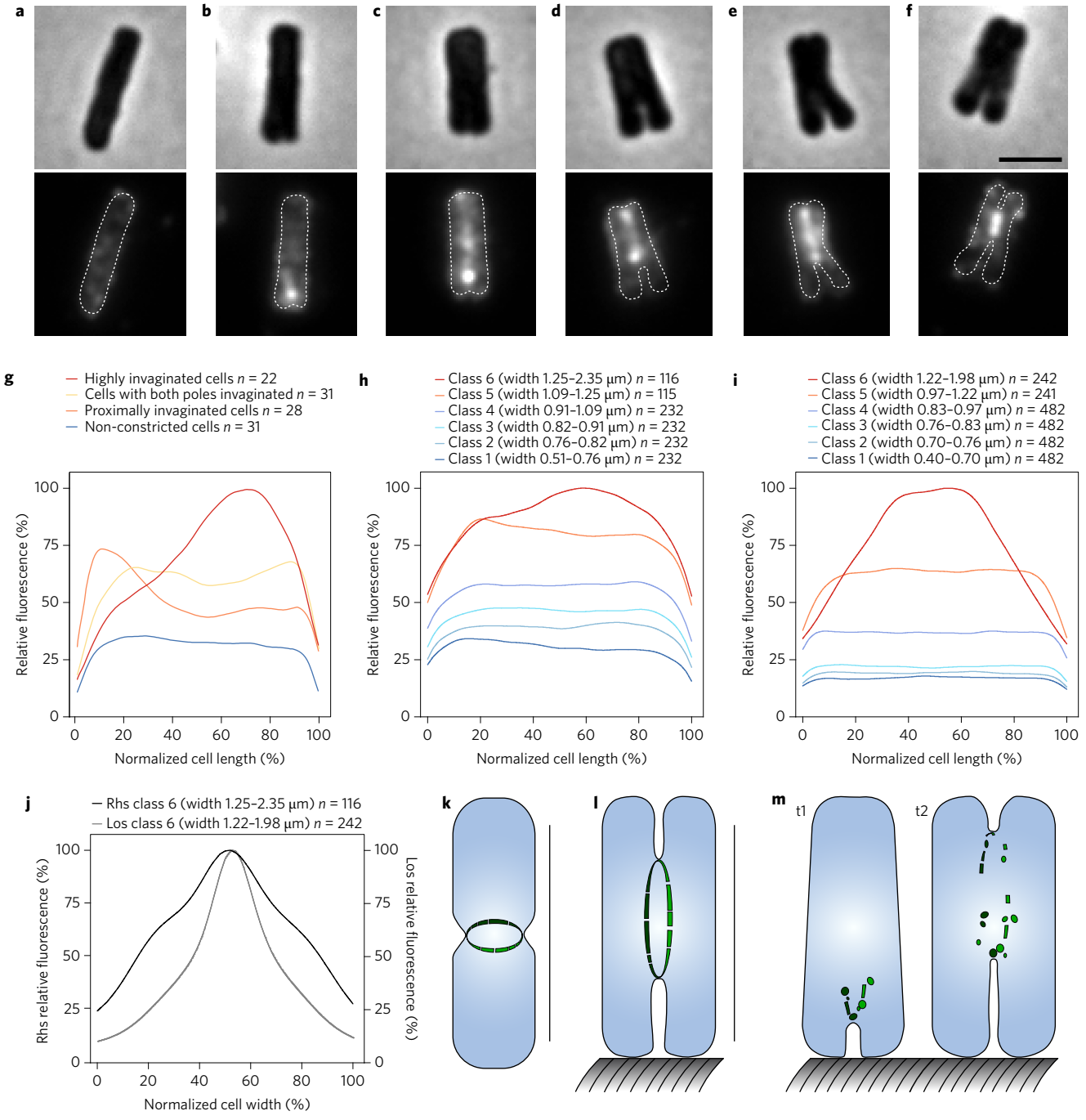

Figure 2 | Rhs FtsZ localization pattern. a–f, Representative phase contrast (upper panels) and epifluorescence micrographs (lower panels) of Rhs cells immunostained with anti-FtsZ antibody: a non-dividing cell (**a**), a proximally invaginated cell (**b**,**c**) and proximally and distally invaginated cells (**d**–**f**, early to late stages of septation are arranged from left to right). The results are representative of a minimum of five independent experiments. Scale bar, 2 µm. **g**, FtsZ total fluorescence plotted against cell length of Rhs cells grouped into four classes according to their morphology. Average fluorescence profiles of non-dividing cells (blue line; $n = 31$), cells with one invaginating (proximal) pole (orange line; $n = 28$), cells with highly invaginated proximal pole and indented distal pole (yellow line; $n = 31$) and cells with two invaginating poles (red line; $n = 22$). FtsZ fluorescence is expressed in relative fluorescence (%) and plotted against cell length (expressed as a percentage). The results are representative of a minimum of five independent experiments. **h**, FtsZ fluorescence plotted against cell length of Rhs cells ($n = 1,159$) arbitrarily grouped into six size classes. The fluorescence signal of each class was binned into one average fluorescent profile. FtsZ fluorescence is expressed in relative fluorescence (%) and plotted along the cell length (expressed as a percentage). The results are representative of a minimum of five independent experiments. **i**, FtsZ fluorescence plotted against cell length of Los cells ($n = 2,411$) arbitrarily grouped into six size classes. The fluorescence signal of each class was binned into one average fluorescent profile. FtsZ fluorescence is expressed as relative fluorescence (%) and plotted along the cell length (expressed as a percentage). The results are representative of a minimum of five independent experiments. **j**, Average FtsZ fluorescence profile of the widest Rhs (black) and Los (grey) cells (corresponding to size class 6 of Supplementary Fig. 11a,b, respectively) expressed in relative fluorescence (%) and plotted along the cell width (expressed as a percentage). The results are representative of a minimum of five independent experiments. **k**–**m**, Schematic representation of FtsZ-mediated fission in *E. coli*, Los and Rhs: *E. coli* (**k**), Los (**l**) and proximally invaginated Rhs (t1, corresponding to **b**) and proximally and distally invaginated Rhs (t2, corresponding to **d**) (**m**). FtsZ is depicted in green.

with an anti-*E. coli* FtsZ antibody (Supplementary Figs 3b and 12) and immunostained Rhs FtsZ (Fig. 2a–f and Supplementary Figs 5–8). Moreover, we measured the total FtsZ fluorescence of cells belonging to the same morphological or size class (Fig. 2g,h, $n = 112$ and 1,159, respectively) and plotted it against cell length expressed in percentage. In cells showing no sign of membrane invagination (Fig. 2a and blue lines in Fig. 2g,h), FtsZ is homogeneously distributed throughout the cell. In cells only proximally, but not distally invaginated (Fig. 2b,c), FtsZ accumulates in the proximal ~10% of the cell (orange lines in Fig. 2g,h). In cells having both poles invaginated (Fig. 2d,e), the FtsZ signal is localized to the distal half of the cell (yellow line in Fig. 2g). In the final stage of division (Fig. 2f and red line in Fig. 2g,h; standard deviation for all profiles is shown in Supplementary Fig. 9), the FtsZ signal is maximal and localized to the distal 30% of the Rhs cell, the last membrane region to ingress. Notably, no proximal-to-distal shift in FtsZ localization is observable in another longitudinally dividing symbiont (Los; Fig. 2i). Here, and as previously shown[1], the FtsZ fluorescence is either homogeneously distributed throughout the cell length (blue and orange lines in Fig. 2i) or it accumulates at midcell (that is, the axis running from the centre of the proximal pole to the centre of the distal pole) as shown by the single peak (Fig. 2i, red line). In conclusion, a proximal-to-distal shift in FtsZ concentration mediates Rhs asynchronous, longitudinal fission by default.

Given the asynchronicity of Rhs fission and the proximal-to-distal shift of FtsZ concentration in dividing cells, we hypothesized that FtsZ must not be arranged into a ring to mediate cell division at any cell cycle stage. To test our hypothesis, we made confocal laser scanning microscopy (CLSM)-based 3D reconstructions of its expression pattern in cells at late septation stages. A continuous ring-like structure could not be detected in cells displaying both a proximal and apical FtsZ signal (Supplementary Fig. 10 and Supplementary Videos 1–3). At the cell population level, the presence of FtsZ outside the Rhs septation plane is evident by plotting the total FtsZ fluorescence of deeply invaginated cells along the cell width (black line in Fig. 2j and red line in Supplementary Fig. 11a): two fluorescence 'shoulders' accompany the midcell peak in the Rhs FtsZ trace, but not in the Los trace (grey line in Fig. 2j and red line in Supplementary Fig. 11b).

Our fluorescence microscopy studies of fixed Rhs cells indicate that cell envelope invagination does not require native FtsZ to form a ring-like structure at any division stage. Instead, Rhs longitudinal fission appears to proceed by sequential, local FtsZ-mediated membrane invagination, supporting the patchy band model. Although super-resolution imaging indicated the same for *Caulobacter crescentus* and *E. coli*, both studies made use of fluorescent fusion proteins[11,25]. The present study is the first based on immunofluorescence microscopy, which shows that a ring-like structure is dispensable for FtsZ-based bacterial fission at every septation stage (Fig. 2k–m). Non-ring FtsZ-mediated invagination has been observed in the cyanelles of the glaucophyte *Cyanophora paradoxa*[26] and spherical *E. coli*[27]. In *C. paradoxa* and the *rod*A mutant KLB24, septation starts from a single point of the sphere, with localized invagination growing further outward and eventually encompassing the whole cell[26,28]. FtsZ shows a similar pattern: it starts to localize as a single point, which grows into arcs and eventually forms a complete ring[26–28]. In contrast to these findings, in Rhs, FtsZ does not nucleate from a single point only (Fig. 2k–m) and a fully formed ring cannot be observed. Rhs is the first rod-shaped bacterium and the first gammaproteobacterium in which asynchronous septation, mediated by multiple, sequential FtsZ foci, is the default division mechanism. In the absence of a continuous FtsZ ring it is hard to imagine mechanisms for the generation of a sustained constrictive force. Instead, a model where a transient constrictive force mediates local membrane pinching seems to better fit the available experimental data. Such a model may be the already proposed 'iterative pinching model'[29], which postulates that membrane-bound FtsZ protofilaments provide a constrictive force by undergoing a guanosine triphosphate hydrolysis-driven transition to a highly curved conformation, followed by filament depolymerization.

Eukaryotic organisms such as legumes and weevils can dramatically influence the cell cycle of their symbionts[3]. Similarly, the nematode host might trigger Rhs polarity and/or septation asynchronicity. In this scenario, the asynchronous division of Rhs may be an adaptation to its symbiotic lifestyle. Widening cell biological studies to non-model bacteria may greatly advance the understanding of how FtsZ drives cell division. FtsZ is not only almost ubiquitously essential for this fundamental process, but it is a key next-generation antibiotic target[30].

Methods

Ectosymbiont collection and *E. coli* strain. Sediment samples were collected on multiple field trips (2011–2015) at ~1 m depth from a sand bar off Carrie Bow Caye, Belize (16°48′11.01″N, 88°4′54.42″W). Specimens of *R. hypermnestra* and *L. oneistus* were extracted from the sediment by stirring the sand in seawater and pouring the supernatant through a 63 µm mesh sieve. The retained material was transferred into a Petri dish, and single nematodes were handpicked using pipettes under a dissecting microscope. *R. hypermnestra* was identified according to ref. 16. For DNA extraction, western blotting and immunostaining, nematodes were fixed in methanol and transported and stored at −20 °C. For scanning electron microscopy (SEM) the samples were fixed according to ref. 31 with PIPES/HEPES/EGTA/magnesium chloride-buffered glutaraldehyde (2.5%) overnight at 4 °C, rinsed twice with washing buffer and transported and stored in washing buffer at 4 °C. The wild-type *E. coli* K12 strain MC4100 was grown to steady state in minimal glucose medium, kept at 28 °C and agitated during fixation before collection by centrifugation[32].

SEM. Whole worms were post-fixed with 1% osmium tetroxide for 2 h at 4 °C. Bacteria were dissociated from the nematodes by sonication, and the supernatant was transferred on a glass slide coated with poly-L-lysine for attachment, before post-fixation as described above. The samples were further dehydrated with a graded ethanol series, followed by pure acetone and critical point drying with a CPD 300 unit (Leica). Finally, they were mounted on stubs and gold coated with an AGAR B7340 sputtercoater unit. Images were acquired with a XL20 (Philips) using the Microscope control program (version 7.00, FEI) and a Quanta FEG 250 scanning electron microscope (FEI) using the xT microscope control software version 6.2.6.3123.

DNA extraction and homology cloning of *R. hypermnestra* ectosymbiont *ftsZ* gene. Genomic DNA was extracted from three single *R. hypemnestra* nematodes as previously described[33], and 2 µl were used as DNA template in each 50 µl PCR reaction. A 1,438-nucleotide (nt)-long fragment was amplified using specific Rhs *ftsZ* genes primers RhsftsZ2016F (5′-CCATCGAGCAAAACGGGAGA-3′) and RhsftsZ2016R (5′-CGAAGAGGCTGTTGTGCTGA-3′). PCR conditions were as follows: 95 °C for 5 min, followed by 33 cycles at 95 °C for 45 s, 57 °C for 45 s, 72 °C for 95 s, followed by a final elongation step at 72 °C for 10 min. We randomly picked and fully sequenced six clones containing the *R. hypemnestra* symbiont *ftsZ* gene fragment in both directions. Sequences were aligned and compared with CodonCode Aligner 3.7.1 software (CodonCode Corporation).

Western blot. For western blots, proteins from dissociated ectosymbionts were separated by reduced SDS–polyacrylamide gel electrophoresis (PAGE) on NuPAGE 4–12% Bis-Tris pre-cast gels (Invitrogen), followed by transfer to Hybond ECL nitrocellulose membranes (Amersham Biosciences). Membranes were blocked for 45 min in PBS containing 5% (wt/vol) nonfat milk (PBSM) at room temperature and incubated overnight at 4 °C with either a rabbit polyclonal anti-*E. coli* FtsZ antibody[34] (1:400 dilution) or a sheep polyclonal anti-*E. coli* pili antibody (ab35292, Abcam) raised against *E. coli* K88 fimbrial protein AB/FaeG (http://www.uniprot.org/uniprot/P02970; 1:1,000 dilution) in PBSM. For the negative control, the primary antibody was omitted at this step. After three washing steps in PBSM to remove unbound antibody, the blots were incubated for 1 h at room temperature with a horseradish peroxidase-conjugated anti-rabbit or anti-sheep secondary antibody (1:5,000, Amersham Biosciences) in PBSM. Protein–antibody complexes were visualized using ECL Plus detection reagents and films (Amersham Biosciences).

Immunostaining. Fixed nematodes were rehydrated and washed in PBS containing 0.1% Tween 20 (PBT), followed by permeabilization of the bacterial peptidoglycan by incubation for 10 min with 0.1% (wt/vol) lysozyme at 37 °C (lysozyme incubation was omitted for anti-pili antibody immunostaining). Blocking was carried out for 1 h in PBT containing 2% (wt/vol) bovine serum albumin (blocking solution) at

room temperature. Rhs were immunostained with a 1:500 dilution of rabbit polyclonal anti-*E. coli* FtsZ antibody[34] or with a 1:200 dilution of sheep polyclonal anti-*E. coli* pili antibody in blocking solution overnight at 4 °C. For the negative control, the primary antibody was omitted for this step. The samples were washed three times in PBT to remove unbound primary antibody and incubated with secondary Alexa488 conjugated anti-rabbit (Jackson ImmunoResearch) for anti FtsZ and Alexa555 conjugated anti-sheep antibody (Thermo Fisher Scientific) for anti-K88ab at 1:500 dilution in blocking solution for 1 h at room temperature. Los FtsZ immunostaining was performed according to ref. 1. Unbound secondary antibody was removed by three washing steps in PBT, and worms were sonicated for 40 s in the tubes to dissociate Rhs before mounting. A 1 µl volume of the bacterial solution was mixed with 0.5 µl of mounting medium Vectashield (Vector Labs).

Cell size and fluorescence measurements. Cell suspensions were applied on a 1% agarose-covered microscopy slide[35] and imaged using a Nikon Eclipse 50i microscope equipped with either a DS-Fi1 camera (Nikon) or an MFCool camera (Jenoptik). Epifluorescence images were acquired using the NIS Elements F 3.22 software (Nikon) or the ProgRes Capture Pro 2.8.8 software (Jenoptik) and processed using the public domain program ImageJ (ref. 36) in combination with plugin ObjectJ and a modified version of Coli-Inspector[34,37]. Cell outlines were automatically traced and cell length, width and fluorescence patterns were measured. Automatic cell recognition was manually double-checked in order to remove remaining errors. The morphological information from the phase contrast was used to automatically assign polarity to the cells. The proximal pole is wider because the division starts there, so the poles were measured and the wider pole assigned as proximal then manually double-checked. For the length- and width-based average fluorescence profile (Fig. 2 h–j; Supplementary Fig. 11), Rhs and Los were divided into six classes of increasing width (classes 1–4 contain 20% of the cells and classes 5 and 6 contain 10% of the cells each), and the fluorescence signal of each binned class was averaged into one fluorescent profile. For Rhs the width classes were 0.51–0.76 µm, 0.76–0.826 µm, 0.826–0.914 µm, 0.914–1.09 µm, 1.09–1.25 µm and 1.25–2.35 µm. For Los these were 0.4–0.705 µm, 0.705–0.767 µm, 0.767–0.837 µm, 0.837–0.972 µm, 0.972–1.22 µm and 1.22–1.98 µm. For the average fluorescence plot (Fig. 2g and Supplementary Fig. 9), cells were chosen based on phase-contrast images, the length was standardized, and the fluorescence intensities were added up and averaged. Three-dimensional images of the cells were obtained using a CLSM (Nikon A1), using a ×60 oil objective (NA 1.4) and excitation with a 488 nm laser for the anti FtsZ. The pinhole was set to 1 AU. Step size was 0.100 µm, and 41 steps were taken so that 4 µm in the *z* direction was imaged. The pixel size was 0.050 µm. The point spread function was determined using beads (Tetraspeck Microspheres, Thermo Fisher Scientific) with 200 nm diameter using the same illumination conditions as for the cells. Deconvolution was performed using Huygens software (Scientific Volume Imaging). The animations of the three-dimensional models were created with the visualization software Amira 6.0.1 (FEI). Initially, transmitted light and deconvoluted fluorescence microscopy images were co-registered in three-dimensional space. The volume of the transmitted light images served as a template for segmentation and surface mesh generation for the cellular envelope. The deconvoluted fluorescent signals inside the cell were visualized by false-colour volume renderings. Thresholding of the volume renderings was adjusted to exclude noise and fluorescent artefacts. Data analysis was performed using Excel 2010 (Microsoft Corporation) and SigmaPlot 12.0.0.182 (Systat Software). Graphs were created with SigmaPlot and figures were compiled using Photoshop CS6 and Illustrator CS 6 (Adobe Systems).

Data availability. The Rhs *ftsZ* open reading frame has been deposited in GenBank under accession no. KU847423 (BankIt1897148).

Received 18 March 2016; accepted 26 August 2016; published 10 October 2016

References

1. Leisch, N. *et al. Curr. Biol.* **22,** R831–R832 (2012).
2. Pende, N. *et al. Nat. Commun.* **5,** 4803 (2014).
3. Bulgheresi, S. *Environ. Microbiol.* **18,** 2305–2318 (2016).
4. Margolin, W. *Nat. Rev. Mol. Cell Biol.* **6,** 862–871 (2005).
5. Bi, E. F. & Lutkenhaus, J. *Nature* **354,** 161–164 (1991).
6. Adams, D. W. & Errington, J. *Nat. Rev. Microbiol.* **7,** 642–653 (2009).
7. de Boer, P. A. *Curr. Opin. Microbiol.* **13,** 730–737 (2010).
8. Erickson, H. P., Anderson, D. E. & Osawa, M. *Microbiol. Mol. Biol. Rev.* **74,** 504–528 (2010).
9. Mingorance, J., Rivas, G., Vélez, M., Gómez-Puertas, P. & Vicente, M. *Trends Microbiol.* **18,** 348–356 (2010).
10. Osawa, M. & Erickson, H. P. *Proc. Natl Acad. Sci. USA* **110,** 11000–11004 (2013).
11. Coltharp, C., Buss, J., Plumer, T. M. & Xiao, J. *Proc. Natl Acad. Sci. USA* **113,** E1044–E1053 (2016).
12. Milam, S. L., Osawa, M. & Erickson, H. P. *Biophys. J.* **103,** 59–68 (2012).
13. Szwedziak, P., Wang, Q., Bharat, T. A., Tsim, M. & Lowe, J. *eLife* **3,** 642 (2014).
14. Haeusser, D. P. & Margolin, W. *Nat. Rev. Microbiol.* **14,** 305–319 (2016).
15. Bayer, C. *et al. Environ. Microbiol. Rep.* **1,** 136–144 (2009).
16. Ott, J. A., Gruber-Vodicka, H. R., Leisch, N. & Zimmermann, J. *Syst. Biodivers.* **12,** 434–455 (2014).
17. Klemm, P. *Eur. J. Biochem.* **117,** 617–627 (1981).
18. Bakker, D., Willemsen, P. T., Simons, L. H., van Zijderveld, F. G. & de Graaf, F. K. *Mol. Microbiol.* **6,** 247–255 (1992).
19. Xia, P., Song, Y., Zou, Y., Yang, Y. & Zhu, G. *J. Basic Microbiol.* **55,** 1118–1124 (2015).
20. Westerlund-Wikström, B. & Korhonen, T. K. *Int. J. Med. Microbiol.* **295,** 479–486 (2005).
21. Krogfelt, K. A. *Rev. Infect. Dis.* **13,** 721–735 (1991).
22. Sung, M. A., Fleming, K., Chen, H. A. & Matthews, S. *EMBO Rep.* **2,** 621–627 (2001).
23. Van den Broeck, W., Cox, E., Oudega, B. & Goddeeris, B. M. *Vet. Microbiol.* **71,** 223–244 (2000).
24. Van Gerven, N., De Greve, H. & Hernalsteens, J. P. *A. Van Leeuw. J. Microb.* **93,** 219–226 (2008).
25. Holden, S. J. *et al. Proc. Natl Acad. Sci. USA* **111,** 4566–4571 (2014).
26. Sato, M. *et al. Planta* **229,** 781–791 (2009).
27. Zaritsky, A. *et al. Biochimie* **81,** 897–900 (1999).
28. Addinall, S. G. & Lutkenhaus, J. *Mol. Microbiol.* **22,** 231–237 (1996).
29. Li, Z., Trimble, M. J., Brun, Y. V. & Jensen, G. J. *EMBO J.* **26,** 4694–4708 (2007).
30. den Blaauwen, T., Andreu, J. M. & Monasterio, O. *Bioorg. Chem.* **55,** 27–38 (2014).
31. Montanaro, J., Gruber, D. & Leisch, N. *PeerJ* **4,** e1860 (2016).
32. den Blaauwen, T., Aarsman, M. E. G. Vischer, N. O. E. & Nanninga, N. *Mol. Microbiol.* **47,** 539–547 (2003).
33. Schizas, N. V., Street, G. T., Coull, B. C., Chandler, G. T. & Quattro, J. M. *Mol. Mar. Biol. Biotech.* **6,** 381–383 (1997).
34. Vischer, N. O. *et al. Front. Microbiol.* **6,** 586 (2015).
35. Koppelman, C. *et al. Mol. Microbiol.* **51,** 645–657 (2004).
36. Schneider, C. A., Rasband, W. S. & Eliceiri, K. W. *Nat. Meth.* **9,** 671–675 (2012).
37. van der Ploeg, R. *et al. Mol. Microbiol.* **87,** 1074–1087 (2013).

Acknowledgements

This work was supported by the Austrian Science Fund (FWF) project P22470 (N.L. and S.B.), a uni:docs fellowship from the University of Vienna (N.P.), PhD completion grant 2014 of the University of Vienna (N.L.), the Max Planck Society (N.L. and H.R.G-V.), an ERC grant (N.L.) and by FWF project P28593 (P.M.W.). The authors acknowledge the Cell Imaging and Ultrastructure Research Core Facility of the University of Vienna and the Van Leeuwenhoek Centre for Advanced Microscopy of the University of Amsterdam for technical support. The authors thank J. A. Ott for providing some of the specimens, M. Loose and three anonymous reviewers for helping to improve the manuscript, and the Department of Ecogenomics & Systems Biology (University of Vienna) for inspiring discussions. This work is contribution 991 from the Carrie Bow Cay Laboratory, Caribbean Coral Reef Ecosystem Program, National Museum of Natural History, Washington DC.

Author contributions

N.L. conceived and designed some of the experiments, performed experiments, analysed the data, contributed materials and wrote a first draft of the paper. N.P. performed experiments, analysed the data, contributed materials. P.M.W. performed experiments and analysed the data. H.R.G.V. contributed materials. J.V. performed experiments. N.V. and S.S.A. contributed analysis tools. B.G. analysed the data. T.d.B. analysed the data, contributed analysis tools, and assessed and commented on the results and conclusions. S.B. conceived and designed the study, contributed materials and wrote the paper.

Additional information

Supplementary information is available for this paper.

Reprints and permissions information is available at www.nature.com/reprints.

Correspondence and requests for materials should be addressed to S.B.

How to cite this article: Leisch, N. *et al.* Asynchronous division by non-ring FtsZ in the gammaproteobacterial symbiont of *Robbea hypermnestra*. *Nat. Microbiol.* **2,** 16182 (2016).

Competing interests

The authors declare no competing financial interests.